Multiparticle azimuthal correlations in p-Pb and Pb-Pb collisions at the CERN Large Hadron Collider

(ALICE Collaboration) Abelev, B.; ...; Antičić, Tome; ...; Gotovac, Sven; ...; Mudnić, Eugen; ...; Planinić, Mirko; ...; ...

Source / Izvornik: **Physical Review C - Nuclear Physics, 2014, 90**

Journal article, Published version
Rad u časopisu, Objavljena verzija rada (izdavačev PDF)

https://doi.org/10.1103/PhysRevC.90.054901

Permanent link / Trajna poveznica: https://urn.nsk.hr/urn:nbn:hr:217:515253

Multiparticle azimuthal correlations in *p*-Pb and Pb-Pb collisions at the CERN Large Hadron Collider

B. Abelev *et al.*[*]
(ALICE Collaboration)

(Received 11 June 2014; revised manuscript received 16 September 2014; published 3 November 2014)

Measurements of multiparticle azimuthal correlations (cumulants) for charged particles in p-Pb at $\sqrt{s_{\rm NN}} = 5.02$ TeV and Pb-Pb at $\sqrt{s_{\rm NN}} = 2.76$ TeV collisions are presented. They help address the question of whether there is evidence for global, flowlike, azimuthal correlations in the p-Pb system. Comparisons are made to measurements from the larger Pb-Pb system, where such evidence is established. In particular, the second harmonic two-particle cumulants are found to decrease with multiplicity, characteristic of a dominance of few-particle correlations in p-Pb collisions. However, when a $|\Delta\eta|$ gap is placed to suppress such correlations, the two-particle cumulants begin to rise at high multiplicity, indicating the presence of global azimuthal correlations. The Pb-Pb values are higher than the p-Pb values at similar multiplicities. In both systems, the second harmonic four-particle cumulants exhibit a transition from positive to negative values when the multiplicity increases. The negative values allow for a measurement of $v_2\{4\}$ to be made, which is found to be higher in Pb-Pb collisions at similar multiplicities. The second harmonic six-particle cumulants are also found to be higher in Pb-Pb collisions. In Pb-Pb collisions, we generally find $v_2\{4\} \simeq v_2\{6\} \neq 0$ which is indicative of a Bessel-Gaussian function for the v_2 distribution. For very high-multiplicity Pb-Pb collisions, we observe that the four- and six-particle cumulants become consistent with 0. Finally, third harmonic two-particle cumulants in p-Pb and Pb-Pb are measured. These are found to be similar for overlapping multiplicities, when a $|\Delta\eta| > 1.4$ gap is placed.

DOI: 10.1103/PhysRevC.90.054901 PACS number(s): 25.75.−q

I. INTRODUCTION

The primary goal of studies with relativistic heavy-ion collisions is to create the quark gluon plasma (QGP), a unique state of matter where quarks and gluons can move freely over large volumes in comparison to the typical size of a hadron. Studies of azimuthal anisotropy for produced particles have contributed significantly to the characterization of the system created in heavy-ion collisions. These studies are based on a Fourier expansion of the azimuthal distribution given by [1]

$$\frac{dN}{d\varphi} \propto 1 + 2\sum_{n=1}^{\infty} v_n \cos[n(\varphi - \Psi_n)], \tag{1}$$

where φ is the azimuthal angle of produced particles. In heavy-ion collisions, the v_n terms generally represent flow coefficients where n is the flow harmonic and Ψ_n is the corresponding flow angle. The flow coefficients are believed to reflect the response of the system to spatial anisotropies in the initial state. Measurements of the second harmonic flow coefficient (v_2, elliptic flow) received keen attention at Relativistic Heavy Ion Collider (RHIC), where the correspondence with hydrodynamic calculations in Au+Au $\sqrt{s_{\rm NN}} = 200$ GeV collisions indicated that an almost perfect liquid had been produced in the laboratory [2–5]. Larger values of integrated v_2 have been observed at the Large Hadron Collider (LHC) in Pb-Pb at $\sqrt{s_{\rm NN}} = 2.76$ TeV collisions, indicating that the system created at this new energy regime still behaves as an almost ideal liquid [6]. While the initial state anisotropy is usually dominated by an elliptical overlap area which gives rise to v_2, measurements of the third harmonic flow (v_3, triangular flow) demonstrated initial state fluctuations modulate the overlap area, and they provide additional constraints to the transport coefficients of the system (e.g., the value of the shear viscosity over entropy ratio η/s) [7–11]. The combination of the second and higher harmonic flow coefficients manifest themselves in two-particle correlation structures (along $\Delta\eta$) such as the away-side double hump ($\Delta\varphi \sim \pi$), and near-side ridge ($\Delta\varphi \sim 0$) observed both at RHIC and the LHC.

The study of p-Pb collisions, which usually provides baseline measurements for the quantification of cold nuclear matter effects, led to a number of unexpected results [12–18]. The CMS Collaboration reported the development of a near-side ridgelike structure in high-multiplicity p-Pb collisions [12,16]. We discovered a symmetric double ridge structure on both the near and the away side after subtracting from the high-multiplicity p-Pb correlation function the dominant jet contribution using the low multiplicity events [13]. The ATLAS Collaboration confirmed the appearance of such structure using a similar subtraction technique [14]. We extended the measurements to identified hadrons and reported a mass ordering in the $p_{\rm T}$ differential v_2 measurements for the different species, with a crossing of p and π v_2 at large $p_{\rm T}$ [17]. Around a similar time, the CMS and ATLAS Collaborations measured finite values of v_2 from four particle correlations [15,16].

The origin of the ridge structure in p-Pb collisions has been the subject of speculation within the heavy-ion community [19–22]. It has been suggested that a high enough energy density is achieved in p-Pb at $\sqrt{s_{\rm NN}} = 5.02$ TeV collisions

[*]Full author list given at the end of the article.

to induce hydrodynamic flow using a lattice QCD equation of state [19]. Combined with spatial anisotropies in the initial p-Pb state, this mechanism would induce global correlations of soft particles with significant values of v_2 and v_3. A second proposal is that the ridge arises from collimated (in $\Delta\varphi$) correlated two-gluon production from the color glass condensate (CGC) [20]. This leads to few-particle correlations, rather than a global modulation of soft particles. Finally, the third explanation invokes the CGC initial state with a finite number of sources that form the eccentricity [21]. In contrast to the previous explanation, this approach allows for nonzero values of v_2 from four-, six-, and eight-particle correlations in high multiplicity p-Pb collisions.

Whether the current measurements in high-multiplicity p-Pb events reveal the onset of collective behavior, or can be explained in terms of few-particle correlations (i.e., nonflow), is the main goal of this analysis. We report the multiplicity dependence of the two-, four-, and six-particle correlations (cumulants) for charged particles, that can be used as a tool to investigate multiparticle correlations of various harmonics [23,24]. We present the results in both p-Pb and Pb-Pb collisions at $\sqrt{s_{\rm NN}} = 5.02$ TeV and $\sqrt{s_{\rm NN}} = 2.76$ TeV respectively. The multiplicity dependence of these measurements will help decipher how flow and nonflow contribute. In Sec. II, we will introduce multiparticle cumulants and discuss their response to nonflow and flow fluctuations. In Sec. III we will describe the analysis details. Section IV shows our results, and Sec. V presents our summary.

II. MULTIPARTICLE CUMULANTS

The measurements of v_n in Eq. (1) can be done using a variety of methods, which have different sensitivities to flow fluctuations (event-wise variations in the flow coefficients) and nonflow. Nonflow refers to correlations not related to the common symmetry plane Ψ_n, such as those due to resonances and jets. Multiparticle cumulants are utilized since their response to flow fluctuations and nonflow is considered well understood. For a given harmonic n, the average strength of two-particle correlations is determined by forming the following from all pairs:

$$\langle 2\rangle = \langle e^{in(\varphi_1-\varphi_2)}\rangle. \tag{2}$$

The φ values used in the subtraction will originate from different particles to prevent autocorrelations. The single angular brackets denote averaging of particle pairs within the same event. The two-particle cumulant is obtained by averaging $\langle 2\rangle$ over an event ensemble, and is denoted as

$$c_n\{2\} = \langle\langle 2\rangle\rangle. \tag{3}$$

In the absence of nonflow, $c_n\{2\}$ provides a measure of $\langle v_n^2\rangle$ without the need to measure Ψ_n. Respectively, the average strength of four particle correlations is determined by forming the following from all quadruplets:

$$\langle 4\rangle = \langle e^{in(\varphi_1+\varphi_2-\varphi_3-\varphi_4)}\rangle. \tag{4}$$

Consequently, the four-particle cumulant is then

$$c_n\{4\} = \langle\langle 4\rangle\rangle - 2\langle\langle 2\rangle\rangle^2. \tag{5}$$

The subtraction removes nonflow contributions present in two-particle correlations. In the absence of nonflow, $c_n\{4\}$ provides a measure of $\langle v_n^4\rangle - 2\langle v_n^2\rangle^2$. Respectively, the average strength of six-particle correlations is determined by forming the following from all sextuplets:

$$\langle 6\rangle = \langle e^{in(\varphi_1+\varphi_2+\varphi_3-\varphi_4-\varphi_5-\varphi_6)}\rangle. \tag{6}$$

The six-particle cumulant is then

$$c_n\{6\} = \langle\langle 6\rangle\rangle - 9\langle\langle 4\rangle\rangle\langle\langle 2\rangle\rangle + 12\langle\langle 2\rangle\rangle^3. \tag{7}$$

In this case, the subtraction removes nonflow contributions present in two- and four-particle correlations. In the absence of nonflow, $c_n\{6\}$ provides a measure of $\langle v_n^6\rangle - 9\langle v_n^4\rangle\langle v_n^2\rangle + 12\langle v_n^2\rangle^3$. As mentioned earlier, the quantities $\langle 2\rangle$, $\langle 4\rangle$, or $\langle 6\rangle$ can be determined by averaging over all particles in a given event. The quantities can also be determined using the Q-cumulants of different harmonics, which offers a highly efficient method of evaluating multiparticle correlations without having to consider all combinations [24]. The flow coefficients from two-, four-, and six-particle cumulants can finally be obtained from

$$v_n\{2\} = \sqrt{c_n\{2\}}, \tag{8}$$

$$v_n\{4\} = \sqrt[4]{-c_n\{4\}}, \tag{9}$$

$$v_n\{6\} = \sqrt[6]{\frac{1}{4}c_n\{6\}}. \tag{10}$$

If the value of v_n does not fluctuate and there is no nonflow, $v_n\{2\} = v_n\{4\} = v_n\{6\}$. A variation in v_n on an event by event basis leads to differences in each of the values. If the variation is presented with a characteristic standard deviation σ_{v_n}, $v_n\{2\} = \sqrt{\langle v_n\rangle^2 + \sigma_{v_n}^2}$. When $\sigma_{v_n} \ll v_n$, $v_n\{4\} = v_n\{6\} = \sqrt{\langle v_n\rangle^2 - \sigma_{v_n}^2}$ [25,26]. Therefore, the difference in $v_n\{2\}$ and $v_n\{4\}$ can be used to infer the scale of v_n fluctuations σ_{v_n}. The presence of nonflow influences the cumulants as follows. Assuming large multiplicity events are a superposition of low multiplicity events, the contribution from nonflow (or few-particle correlations) is expected to be diluted as [25]

$$c_n\{m\} \propto \frac{1}{M^{m-1}}, \tag{11}$$

where M is the multiplicity of the event. Therefore measuring both $c_n\{2\}$, $c_n\{4\}$, and $c_n\{6\}$ as a function of multiplicity will help determine whether the underlying correlations are global or few-particle. One can also suppress nonflow by requiring the particles to have a relatively large separation in η, since resonances and jets will produce particles with similar rapidity.

III. ANALYSIS DETAILS

The two data sets analyzed were recorded during the p-Pb (in 2013) and the Pb-Pb (in 2010) runs at a center of mass energy of $\sqrt{s_{\rm NN}} = 5.02$ TeV and $\sqrt{s_{\rm NN}} = 2.76$ TeV, respectively. The Pb-Pb run had equal beam energies giving a nucleon-nucleon center of mass system with rapidity $y_{\rm NN} = 0$. However, the p-Pb run had different beam energies per nucleon for the p and Pb beam, and resulted in a center of mass system moving in the laboratory frame with $y_{\rm NN} = 0.465$. All kinematic variables are reported in the laboratory frame. Charged particles are detected using the time projection chamber (TPC), the primary tracking detector of ALICE. The TPC has an angular acceptance of $0 < \varphi < 2\pi$, $|\eta| < 0.9$ for tracks with full radial track length (φ is the azimuthal angle and η is the

pseudorapidity), and $|\eta| < 1.5$ for tracks of reduced length. Information from the inner tracking system (ITS) is used to improve the spatial resolution of TPC tracks, which helps with the rejection of secondary tracks (i.e., not originating from the primary vertex). Primary vertex information is provided by the TPC and the silicon pixel detector (SPD). Two VZERO counters, each containing two arrays of 32 scintillator tiles and covering $2.8 < \eta < 5.1$ (VZERO-A) and $-3.7 < \eta < -1.7$ (VZERO-C), provide information for triggering and event class determination. A more detailed description of the ALICE detector can be found elsewhere [27].

For Pb-Pb collisions, events are selected using a minimum bias trigger, which requires a coincidence of signals in the two VZERO detectors. We use minimum bias and high-multiplicity triggers for p-Pb collisions. As with Pb-Pb, the p-Pb minimum bias trigger requires a coincidence of two signals from the VZERO detectors, and accepts 99.2% of the nonsingle diffractive cross section. The high-multiplicity trigger requires a large number of hits in the SPD. Pile-up events are rejected by removing events with multiple vertices, and ensuring the vertices reconstructed from the TPC and SPD agree within 0.8 cm. After the pile-up rejection procedures, the results are stable with respect to luminosity. Only events with a reconstructed primary vertex within ± 10 cm from the center of the detector along the beam axis are used in the analysis to ensure a uniform acceptance in η. The resulting analyzed event sample consisted of about 110-M p-Pb and 12-M Pb-Pb minimum bias events. In p-Pb collisions, the high-multiplicity trigger allowed for a factor of 10 increase in high-multiplicity events in the top 0.014% of the cross section, compared to the number of minimum bias events. The p-Pb high multiplicity events are used for the last two data points for $n = 2$, and the last data point for $n = 3$. Minimum bias events are used for all other points.

The tracks used to determine the cumulants have kinematic cuts $0.2 < p_T < 3$ GeV/c and $|\eta| < 1$. The tracks use an SPD hit if one exists within the trajectory, if not, they are constrained to the primary vertex. Such a configuration leads to a flat φ acceptance. It was found that residual nonuniformities influence the cumulant extraction at a level of less than 0.1%. We therefore do not apply acceptance corrections. Track quality is ensured by requiring tracks to have at least 70 TPC clusters out of a maximum of 159, and a χ^2 per TPC cluster less than 4 for the track fit. In addition, the distances of closest approach to the primary vertex in the xy plane and z direction are required to be less than 2.4 and 3.2 cm respectively [28].

The results in this article are reported as a function of the corrected multiplicity, $\langle N_{\rm ch}\rangle$. The multiplicity corresponds to the number of charged tracks with $0.2 < p_T < 3$ GeV/c and $|\eta| < 1$, corrected for tracking efficiencies. The tracking efficiency is calculated from a procedure using HIJNG (Pb-Pb) or DPMJET (p-Pb) events [29,30]. GEANT3 is used for transporting simulated particles, followed by a full calculation of the detector response (including production of secondary particles) and track reconstruction done with the ALICE simulation and reconstruction framework [31,32]. The tracking efficiency is ~70% at $p_T \sim 0.2$ GeV/c and increases to an approximately constant value of ~80% for $p_T > 1$ GeV/c. There are differences on the order of a few percent when comparing between the two collision systems due to the change in detector performance between each run. The final number of particles ($\langle N_{\rm ch}\rangle$) is extracted by correcting the raw transverse momentum spectrum with the $p_{\rm T}$ dependent tracking efficiencies. Tables II and III show multiplicities for the two systems and the fractional cross section.

To reduce the influence of the tracking efficiency on the cumulants ($c_n\{m\}$), we flatten the $p_{\rm T}$ dependent efficiencies by randomly rejecting high $p_{\rm T}$ particles. These particles have slightly larger efficiencies compared to the low $p_{\rm T}$ ones, so the procedure effectively reweights the cumulants in favor of low $p_{\rm T}$ particles. This decreases the integrated value of v_n by roughly 3%, since v_n generally increases with $p_{\rm T}$. Regarding the choice of multiplicity bin size, it was previously realized that event by event multiplicity fluctuations within a class having a wide multiplicity range can bias the measurement of $c_n\{4\}$, particularly in the low multiplicity region [16,26]. We avoid this by first extracting $c_n\{m\}$ in unit multiplicity bins (i.e., $N_{\rm ch} = 6,7,8\ldots$). The number of combinations scheme [24] or simple unit event weights gives the same values of $c_n\{m\}$ for unit multiplicity bins. We then average those values to produce $c_n\{m\}$ for larger bin widths, which have a better statistical precision. The following relation is used for averaging procedure: $\langle y\rangle = \frac{\sum_i w_i y_i}{\sum_i w_i}$, where y_i is the value of the cumulant in a single multiplicity bin, w_i corresponds to a choice of weight, and $\langle y\rangle$ is the average value obtained from the number of bins in the sum. Monte Carlo studies with known probability density functions (p.d.f.) show that when using unit weights (i.e. $w_i = 1$), our result lies within $< 0.1\%$ from the known input $\langle y\rangle$ (from the p.d.f.). Other weighting schemes such as $w_i = M$, where M is the multiplicity of the event, or $w_i = 1/\sigma_i^2$ where σ_i is the statistical uncertainty of the bin, gave differences of around 2%.

Additional sources of systematic uncertainties in the calculation of $c_n\{m\}$ were extracted by varying the closest approach to the vertex for the tracks, the cut on the minimum number of TPC clusters, the position of the primary vertex and, finally, by analyzing the event sample separately according to the orientation of the magnetic field.

We also generated events with the AMPT model [33] (which includes flow correlations) that were used as an input to our reconstruction simulations. The cumulants

TABLE I. Summary of systematic uncertainties for p-Pb and Pb-Pb collisions (the acronym n/a stands for nonapplicable).

p-Pb source	$c_2\{2\}$	$c_2\{4\}$	$c_2\{6\}$	$c_3\{2\}$>
Primary vertex position	0.3%	n/a	n/a	0.7%
Track type	2.2%	4.0%	6.0%	2.6%
No. TPC clusters	0.2%	n/a	n/a	0.2%
Comparison to Monte Carlo	1.7%	2.9%	4.5%	3.3%
Total	2.8%	4.9%	7.5%	4.3%
Pb-Pb source	$c_2\{2\}$	$c_2\{4\}$	$c_2\{6\}$	$c_3\{2\}$
Primary vertex position	0.5%	n/a	n/a	n/a
Track type	2.9%	6.1%	9.1%	4.0%
Sign of B-field	0.2%	n/a	n/a	0.2%
Comparison to Monte Carlo	1.7%	2.9%	4.5%	3.3%
Total	3.9%	6.8%	10.2%	5.2%

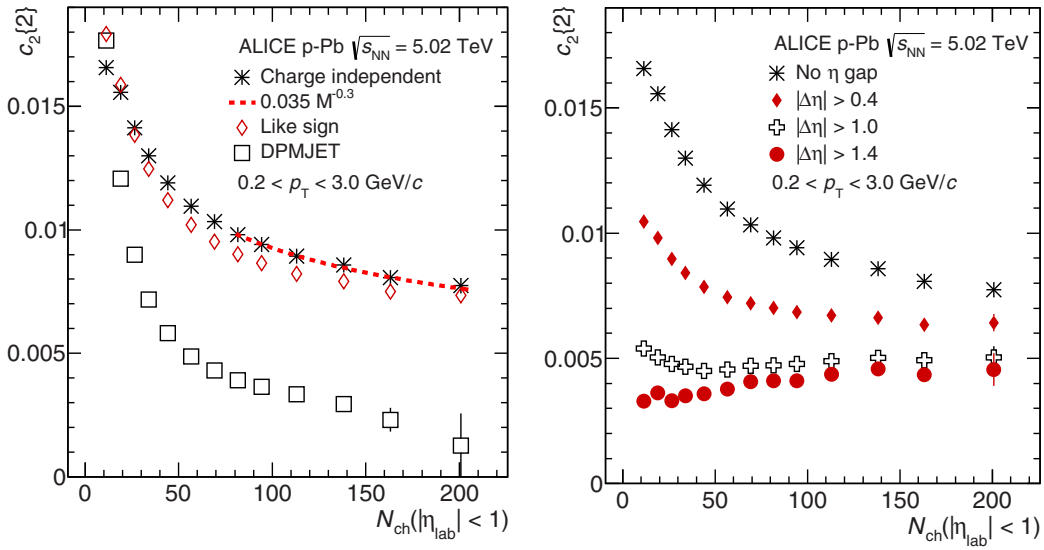

FIG. 1. (Color online) Midrapidity ($|\eta| < 1$) measurements of $c_2\{2\}$ as a function of multiplicity for p-Pb collisions. Only statistical errors are shown as these dominate the uncertainty. See Table I for systematic uncertainties.

obtained directly from the model were compared to those from reconstructed tracks. We found small differences, which are part of the systematic uncertainties. Table I summarizes the systematic uncertainties for each collision system. The final systematic uncertainty is calculated by adding all the individual contributions in quadrature. In the Appendix, Tables II and III show the multiplicities for the two systems and the fractional cross section.

IV. RESULTS

A. The second harmonic two-particle cumulant

The results of $c_2\{2\}$ as a function of multiplicity are shown in Figs. 1 and 2 for p-Pb and Pb-Pb respectively. The left column presents the results, using the Q-cumulants methods [24] in the case where no $\Delta\eta$ gap is applied. Charge independent refers to the fact that all available charged tracks are used to determine the cumulants. The left panel of Fig. 1 shows that the star symbols (charge independent measurements) in p-Pb collisions exhibit a decrease with increasing multiplicity, qualitatively consistent with the expectation of correlations dominated by nonflow effects. When fitting these data points with the function a/M^b at large multiplicity, we find $b = 0.3$. The value $b = 1$ is expected if high-multiplicity events are a linear superposition of low multiplicity events [25]. This deviation from 1 might indicate the existence of another mechanism that increases $c_2\{2\}$, or that the relative fraction of few particle correlations is increasing with multiplicity. In the same plot, we present measurements of like-sign correlations, calculated by measuring $c_2\{2\}$ for positive and negative tracks separately, and

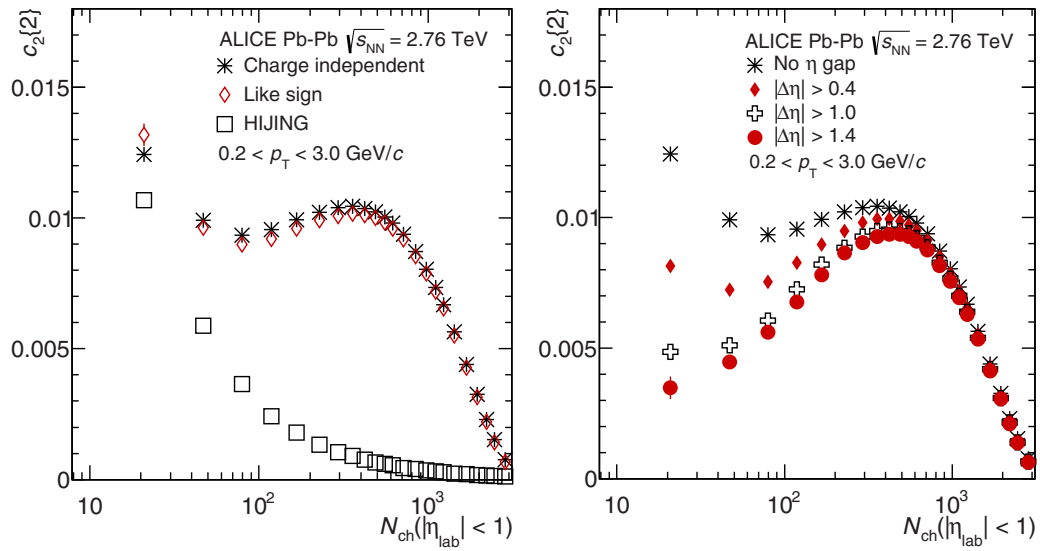

FIG. 2. (Color online) Midrapidity ($|\eta| < 1$) measurements of $c_2\{2\}$ as a function of multiplicity in Pb-Pb collisions. Only statistical errors are shown as these dominate the uncertainty. See Table I for systematic uncertainties.

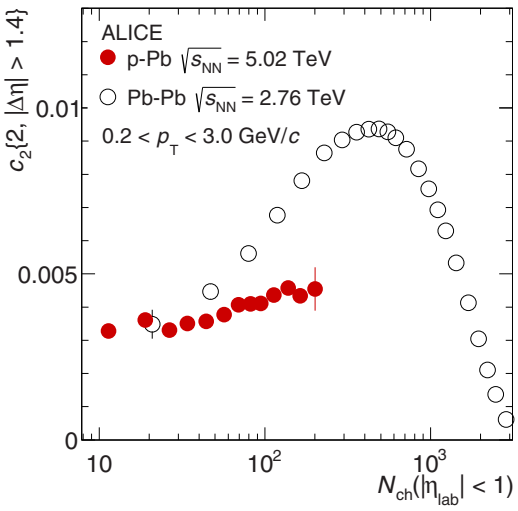

FIG. 3. (Color online) Comparison of $c_2\{2\}$ with $|\Delta\eta| > 1.4$ for p-Pb and Pb-Pb collisions. Only statistical errors are shown as these dominate the uncertainty. See Table I for systematic uncertainties.

forming the average. The corresponding points, represented by the diamonds, are lower than the charge independent results for the majority of the multiplicity ranges. This is expected since few-particle correlations from jets and resonances conserve charge, and thus are more likely to be absent in the like-sign measurements. Conversely, the like-sign measurements are higher for the lowest multiplicity bin. This can be explained by a suppression of unlike sign correlations (e.g., multiparticle jets) induced by the low multiplicity cut. Our results in p-Pb collisions are compared to predictions from the DPMJET model [30]. It includes in a phenomenological way the soft multiparticle production as well as hard scatterings, contains no collective effects and thus can serve as a benchmark to study the effect of nonflow on our measurements. It is seen that the corresponding points for $c_2\{2\}$ in DPMJET fall off more rapidly compared to data. When carrying out the a/M^b fit to the model, we find $b \sim 0.8$. The data is also significantly higher than DPMJET at high multiplicity.

The right panel of Fig. 1 presents the multiplicity dependence of the two-particle cumulants in p-Pb collisions in the case where a $\Delta\eta$ gap is applied. It is seen that for a given multiplicity, increasing the gap decreases $c_2\{2\}$. As mentioned previously, this is expected since tracks from few-particle correlations such as jets and resonances have smaller relative angles, therefore their contribution is suppressed by the applied pseudorapidity separation. However for large $\Delta\eta$ values, i.e., for $|\Delta\eta| > 1$, the data points increase with multiplicity which is not expected if nonflow dominates. In addition, the $|\Delta\eta|$ dependence of $c_2\{2\}$ is less pronounced at higher multiplicities. This could be a consequence of a flowlike mechanism with no or little dependence on η, whose relative strength increases with increasing multiplicity.

The Pb-Pb results of $c_2\{2\}$ in the case of the charge independent and the like-sign analysis are presented in the left panel of Fig. 2. They decrease with increasing multiplicity up to $N_{ch} \sim 100$, then increase until midcentral collisions (i.e., up to $N_{ch} \approx 400$). When moving to more central events where initial state anisotropies decrease, the values of $c_2\{2\}$ decrease as expected. Predictions from the HIJING model are also shown in the same plot. This model, similarly to the DPMJET model, contains only nonflow, and as expected, $c_2\{2\}$ attenuates more rapidly than the data. Finally, the right panel of Fig. 2 presents the two-particle results in Pb-Pb collisions after applying a $\Delta\eta$ gap to reduce the contribution from nonflow. It is seen that at multiplicities $N_{ch} \gtrsim 1000$, the measurements with various $\Delta\eta$ gaps converge, indicating the dominance of anisotropic flow. The measurements at lower multiplicities depend on $\Delta\eta$ gap significantly, indicating nonflow plays a prominent role.

In Fig. 3, we compare $c_2\{2\}$ for p-Pb and Pb-Pb with $|\Delta\eta| > 1.4$ to minimize the contribution from nonflow. Both systems have similar values of $c_2\{2\}$ at low multiplicity, however the Pb-Pb data points rise more rapidly for higher multiplicities.

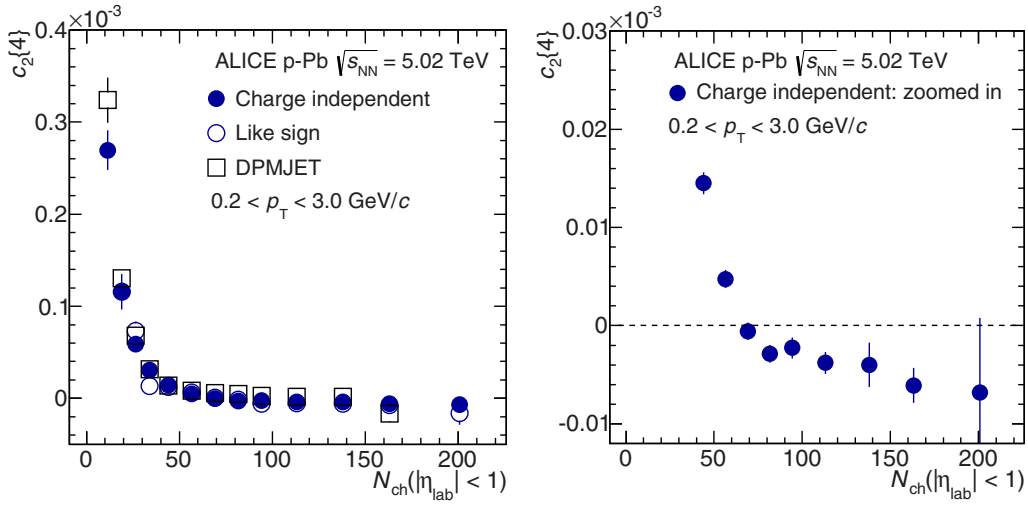

FIG. 4. (Color online) Midrapidity ($|\eta| < 1$) measurements of $c_2\{4\}$ as a function of multiplicity for p-Pb collisions. Only statistical errors are shown as these dominate the uncertainty. See Table I for systematic uncertainties. The right panel shows a zoomed in version of the solid points in the left panel.

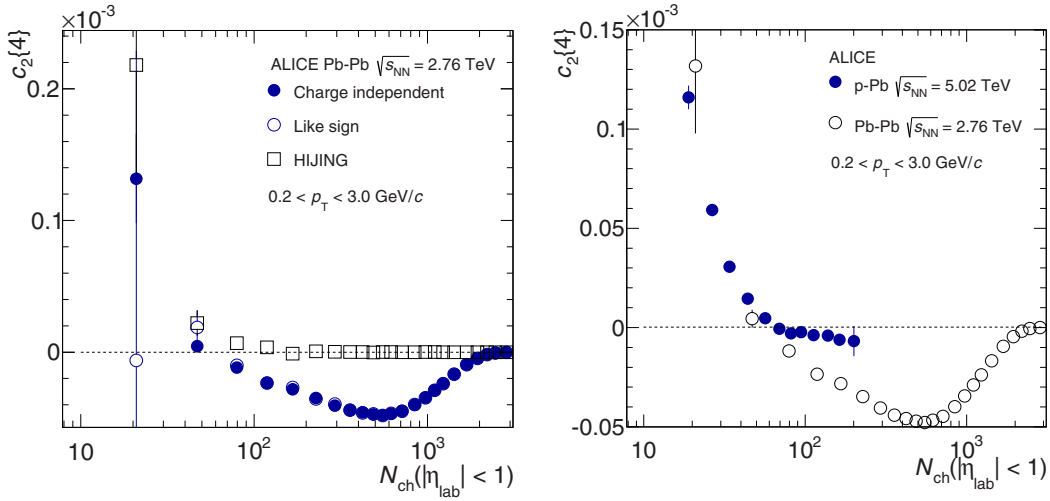

FIG. 5. (Color online) Left panel: Midrapidity ($|\eta| < 1$) measurements of $c_2\{4\}$ as a function of multiplicity for Pb-Pb collisions. Right panel: Comparison of $c_2\{4\}$ for p-Pb and Pb-Pb collisions. Only statistical errors are shown as these dominate the uncertainty. See table I for systematic uncertainties.

This may be explained by higher eccentricities (therefore higher anisotropies) in Pb-Pb collisions found from a CGC inspired cluster model for the initial conditions at similar multiplicities [22] (not shown). We note that other studies are exploring these correlations with the AMPT model [34].

B. The second harmonic four-particle cumulant

The results of $c_2\{4\}$ as a function of multiplicity are shown in Fig. 4 for p-Pb collisions, and Fig. 5 for Pb-Pb collisions. We use the Q-cumulants methods to obtain the results in all cases. For p-Pb collisions, there are little differences between the like-sign and the charge independent results. The values of $c_2\{4\}$ attenuate more rapidly than $c_2\{2\}$ at low multiplicity, as expected since nonflow contributes significantly in this region. The predictions from the DPMJET model, represented by the open squares in Fig. 4, also show a large attenuation. At $N_{\rm ch} \gtrsim 70$, the values of $c_2\{4\}$ become negative, and this is illustrated in the right panel of Fig. 4. Measurements of $c_2\{4\}$ below zero allow for real values of $v_2\{4\}$. We found that the position of the transition from positive to negative depends on the η cut applied to the tracks (not shown). When the η cut is reduced, the transition occurs at a larger multiplicity, which is presumably due to the larger contribution of nonflow. The results for Pb-Pb collisions shown in the left panel of Fig. 5 with the circles exhibit a similar trend. The values of $c_2\{4\}$ rise at very high multiplicities as the collisions become central. The charge independent HIJING predictions, also shown in this plot as open squares, converge to zero for most multiplicities indicating the contribution from nonflow is negligible. In the right panel of Fig. 5, we compare $c_2\{4\}$ for p-Pb and Pb-Pb collisions. Both systems exhibit positive values for $N_{\rm ch} \lesssim 70$, indicating a dominance of nonflow. At multiplicities $70 \lesssim N_{\rm ch} \lesssim 200$, $c_2\{4\}$ decreases more rapidly for Pb-Pb which might be indicative of higher eccentricities for similar multiplicities.

C. The second harmonic six-particle cumulant

The results of $c_2\{6\}$ as a function of multiplicity are shown in Fig. 6 for p-Pb and Pb-Pb collisions. We again use the Q-cumulants methods to obtain $c_2\{6\}$. In p-Pb collisions, these measurements are more limited by finite statistics as we observe fluctuations above and below zero at high multiplicity (within the statistical uncertainties). The solid black line indicates $v_2\{6\} = 4.5\%$, which is roughly the value of $v_2\{4\}$ in this multiplicity region. The p-Pb measurements will benefit from higher statistics measurements planned for future LHC running. However, it is clear at multiplicities above 100 that the values of $c_2\{6\}$ are significantly higher for Pb-Pb compared to p-Pb. This again may be be explained by higher eccentricities in the initial state of the colliding nuclei for the former.

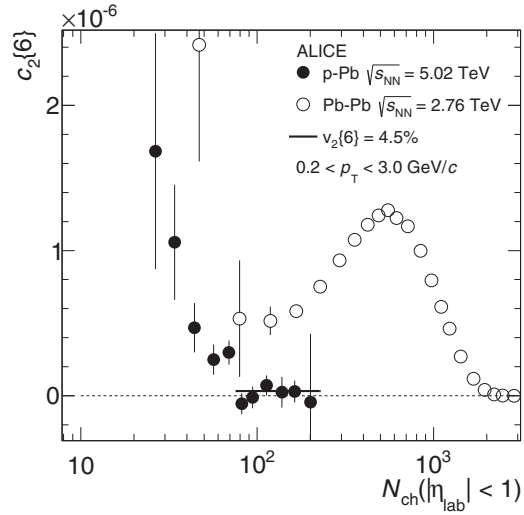

FIG. 6. Comparison of midrapidity ($|\eta| < 1$) $c_2\{6\}$ for p-Pb and Pb-Pb collisions. Only statistical errors are shown as these dominate the uncertainty. See table I for systematic uncertainties.

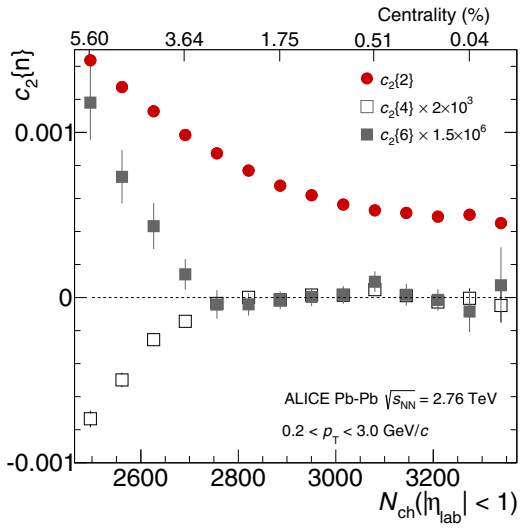

FIG. 7. (Color online) Comparison of $c_2\{m\}$ in very high-multiplicity Pb-Pb collisions. Only statistical errors are shown as these dominate the uncertainty. See Table I for systematic uncertainties.

D. Second harmonic cumulants in very high-multiplicity Pb-Pb collisions

The nonzero values of $c_2\{4\}$ in high-multiplicity p-Pb collisions merit a comparison to high-multiplicity Pb-Pb collisions, which have an impact parameter that becomes small. In both cases, initial state fluctuations are expected to dominate the eccentricity since there is no intrinsic eccentricity from the overlapping nuclei. In Fig. 7, cumulants of different orders are compared for high-multiplicity Pb-Pb collisions. At $N_{ch} \gtrsim 2800$, $c_2\{4\}$ becomes consistent with zero, which is in contrast to high-multiplicity p-Pb (where $c_2\{4\}$ is negative). The measurements of $c_2\{6\}$ also become zero in exactly the same region, which corresponds to the highest ~2.5% of the cross section. Constant fits to $c_2\{4\}$ and $c_2\{6\}$ for $N_{ch} > 2800$ give $8.5 \times 10^{-6} \pm 9.3 \times 10^{-6}$ and $7.2 \times 10^{-6} \pm 2.2 \times 10^{-5}$ respectively (with $\chi^2/dof \sim 1$ in each case). An explanation for the difference between p-Pb and Pb-Pb can be found by considering the number of sources which form the eccentricity. When this number is small, eccentricity fluctuations have a power-law distribution which will lead to finite values of $c_2\{4\}$ and $c_2\{6\}$, assuming $v_2 \propto \varepsilon_2$ [35]. When the number of sources becomes large enough, the power-law distribution becomes equivalent to the Bessel-Gaussian distribution [36,37]. In the special case of very high multiplicity Pb-Pb collisions where the impact parameter is expected to approach 0, the Bessel-Gaussian distribution gives values of $c_2\{4\}$ and $c_2\{6\}$ that are zero. Assuming the number of sources are highly correlated with the number of participants, the difference between very high multiplicity p-Pb and Pb-Pb can be explained by the larger number of sources in the latter. Finally, these results at the LHC can be compared to those from the STAR Collaboration [38,39]. In Au-Au $\sqrt{s_{NN}} = 200$ GeV collisions, $c_2\{4\}$ also approaches zero and may become positive which prevented the extraction of $v_2\{4\}$ in central collisions, while for U-U $\sqrt{s_{NN}} = 193$ GeV collisions, $c_2\{4\}$ always remains negative.

E. Second harmonic flow coefficients in p-Pb and Pb-Pb collisions

A comparison of second harmonic flow coefficients is shown in Fig. 8. We determine $v_2\{2\}$ with the largest possible $\Delta\eta$ gap to minimize the contribution from nonflow. In p-Pb collisions, we find $v_2\{2\} > v_2\{4\}$ which is indicative of flow fluctuations, but can also be affected by nonflow. The same observation is made for Pb-Pb collisions, and we also find $v_2\{4\} \simeq v_2\{6\}$. Regarding the functional form of the v_2 distribution, a Bessel-Gaussian function satisfies the criterium $v_2\{4\} = v_2\{6\}$ [36]. When the Bessel function of the Bessel-Gaussian becomes 1, $v_2\{4\} = v_2\{6\} = 0$. A power-law function gives values of $v_2\{4\}$ and $v_2\{6\}$ which are close, but not exactly equal [35]. In addition, unfolded measurements of

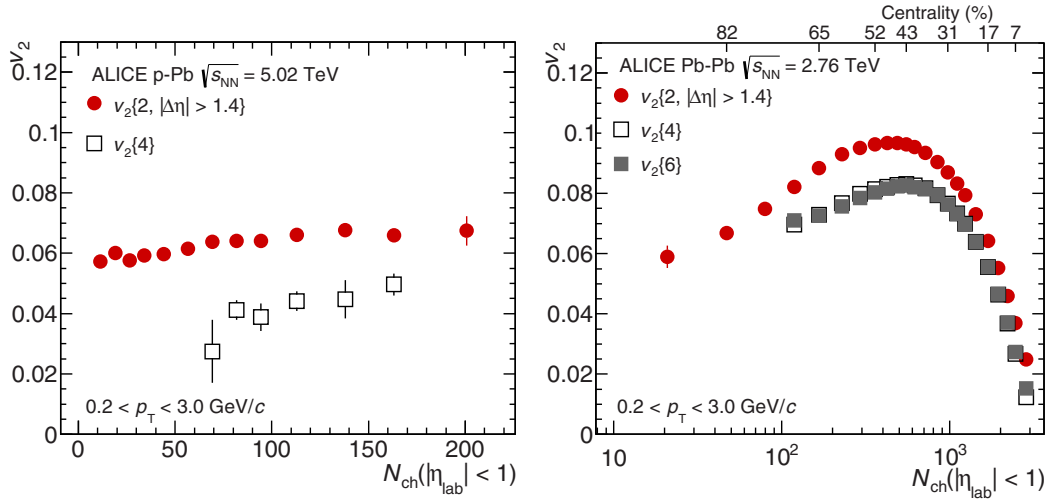

FIG. 8. (Color online) Measurements of $v_2\{2\}$, $v_2\{4\}$, and $v_2\{6\}$ in p-Pb (left panel) and Pb-Pb (right panel) collisions. The measurements of $v_2\{2\}$ are obtained with a $|\Delta\eta| > 1.4$ gap. Only statistical errors are shown as these dominate the uncertainty. See Table I for systematic uncertainties.

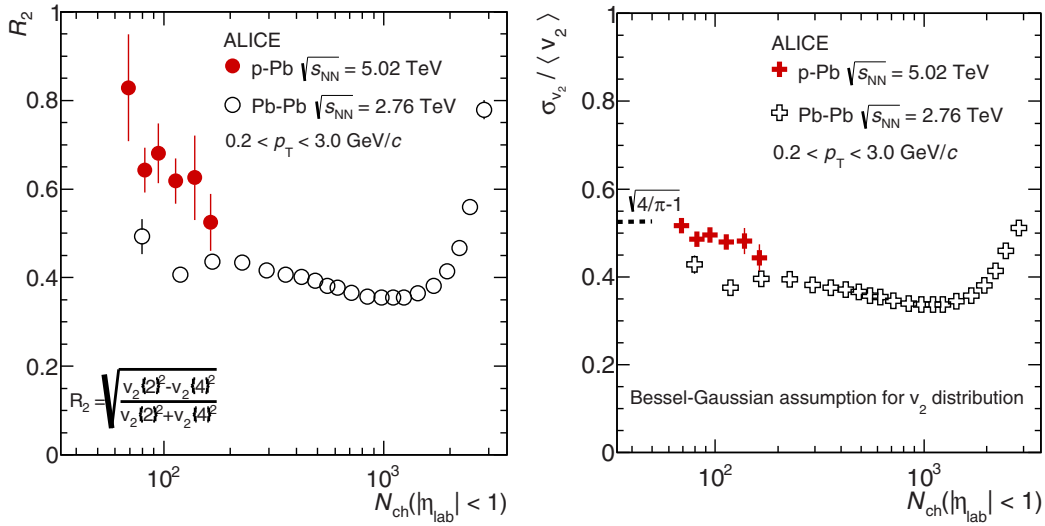

FIG. 9. (Color online) Left panel: Measurements of $[(v_2\{2\}^2 - v_2\{4\}^2)/(v_2\{2\}^2 + v_2\{4\}^2)]^{1/2}$ in p-Pb and Pb-Pb collisions. The measurements of $v_2\{2\}$ are obtained with a $|\Delta\eta| > 1.4$ gap. Only statistical errors are shown as these dominate the uncertainty. See Table I for systematic uncertainties. Right panel: $\sigma_{v2}/\langle v_2 \rangle$ obtained from the same $v_2\{2\}$ and $v_2\{4\}$ measurements assuming a Bessel-Gaussian distribution.

the v_2 distribution have shown Bessel-Gaussian descriptions work reasonably well for Pb-Pb collisions [40,41]. In the left panel of Fig. 9, we show the measurement of R_2, defined as

$$R_n = \sqrt{\frac{v_n\{2\}^2 - v_n\{4\}^2}{v_n\{2\}^2 + v_n\{4\}^2}}. \tag{12}$$

As mentioned in Sec. II, when $\sigma_{v_n} \ll \langle v_n \rangle$, $R_n = \sigma_{v_n}/\langle v_n \rangle$ in case nonflow is negligible. In the overlapping multiplicities, the values for p-Pb appear to be higher than Pb-Pb, demonstrating the greater role of fluctuations in the former. A similar observation is reported by the CMS Collaboration [16]. The trend for R_2 in Pb-Pb is similar to observations for Au-Au $\sqrt{s_{NN}} = 200$ GeV collisions [38,42]. The value of R_2 in mid-central (midmultiplicity) Pb-Pb collisions ($\sim$0.35) is between the STAR and PHOBOS results for similar centralities. In the right panel, we show $\sigma_{v2}/\langle v_2 \rangle$ under the assumption that the v_2 distribution is Bessel-Gaussian. Using this assumption, all the information from distribution can be obtained from just $v_2\{2\}$ and $v_2\{4\}$, without the need for the condition $\sigma_{v_n} \ll v_n$ [36]. The dashed lines denote the $\sigma_{v2}/\langle v_2 \rangle = \sqrt{4/\pi - 1}$ limit, expected when fluctuations dominated the eccentricity [43]. We find that the Bessel-Gaussian $\sigma_{v2}/\langle v_2 \rangle$ is close to this limit for high-multiplicity Pb-Pb collisions.

F. Two-particle cumulants of the third harmonic

In Fig. 10, we show measurements of the third harmonic two-particle cumulants for p-Pb and Pb-Pb collisions, for different values of the $\Delta\eta$ gap. For p-Pb and low Pb-Pb multiplicities, we generally find a strong dependence on the $\Delta\eta$. The values with small $\Delta\eta$ gaps decrease with multiplicity in p-Pb, as expected when nonflow is dominant. This behavior was also observed by the STAR Collaboration at lower beam

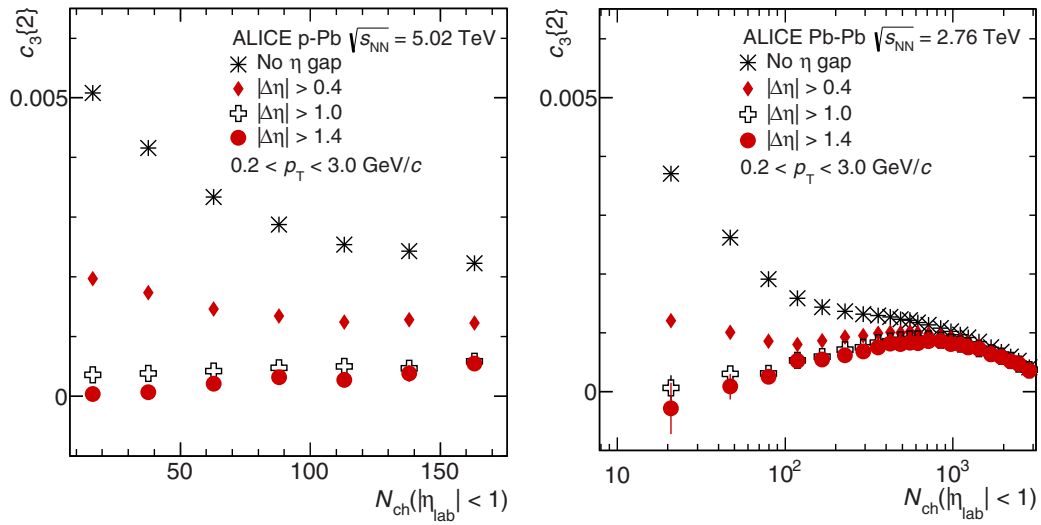

FIG. 10. (Color online) Third harmonic two-particle cumulants in p-Pb and Pb-Pb collisions. Only statistical errors are shown as these dominate the uncertainty. See Table I for systematic uncertainties.

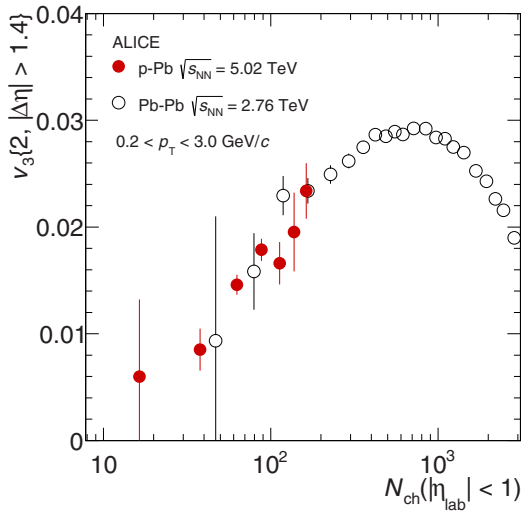

FIG. 11. (Color online) Third harmonic flow coefficients in p-Pb and Pb-Pb collisions. The measurements of $v_3\{2\}$ are obtained with a $|\Delta\eta| > 1.4$ gap. Only statistical errors are shown as these dominate the uncertainty. See Table I for systematic uncertainties.

energies [11]. The measurements with larger $\Delta\eta$ gaps show an increase with multiplicity, indicating a contribution from global correlations. For large Pb-Pb multiplicities, measurements with various $\Delta\eta$ gaps converge indicating a dominance of flow. Finally, in Fig. 11 we compare the third harmonic flow coefficients for both systems, again with the largest possible $\Delta\eta$ gap. In contrast to measurements of the second harmonic, we find that p-Pb and Pb-Pb are consistent for the same multiplicity. This consistency has also been observed by the CMS Collaboration [16], and points to similar third harmonic eccentricities for p-Pb and Pb-Pb at the same multiplicity. A CGC inspired cluster model for the initial conditions is able to reproduce this observation [22].

V. SUMMARY

We have reported results of $c_2\{2\}$, $c_2\{4\}$, and $c_2\{6\}$ as a function of multiplicity in p-Pb at $\sqrt{s_{\rm NN}} = 5.02$ TeV and Pb-Pb at $\sqrt{s_{\rm NN}} = 2.76$ TeV collisions for kinematic cuts $0.2 < p_T < 3$ GeV/c and $|\eta| < 1$. Measurements of $c_2\{2\}$ using all pairs in the event for p-Pb collisions show a decrease with multiplicity, characteristic of a dominance of few-particle correlations. However, the decrease is shallower than from the expectation high-multiplicity events are a superposition of low multiplicity events. When a $|\Delta\eta|$ gap is placed to suppress such nonflow correlations, measurements of $c_2\{2\}$ begin to rise at high multiplicity. Similar observations are made for Pb-Pb collisions. The measurements of $c_2\{4\}$ exhibit a transition from positive values at low multiplicity to negative values at higher multiplicity for both p-Pb and Pb-Pb. The negative values allow for a real $v_2\{4\}$, which is lower than $v_2\{2\}$ at a given multiplicity. The measurements of $c_2\{6\}$ for p-Pb collisions are both consistent with zero, and the assumption $v_2\{4\} = v_2\{6\}$. In Pb-Pb collisions, we observe $v_2\{4\} \simeq v_2\{6\}$, which is indicative of a Bessel-Gaussian function for the v_2 distribution in this domain. For very high-multiplicity Pb-Pb collisions, both $v_2\{4\}$ and $v_2\{6\}$ are consistent with 0. A comparison of p-Pb cumulants to those of Pb-Pb at the same multiplicity (for $N_{\rm ch} \gtrsim 70$) shows stronger correlations in Pb-Pb for all the cumulants. This may be explained by higher eccentricities for similar multiplicities. Finally, we have performed measurements of $v_3\{2\}$ for p-Pb and Pb-Pb collisions. They are found to be similar for overlapping multiplicities when a $|\Delta\eta| > 1.4$ gap is placed, indicating that initial state third harmonic eccentricities may be similar for both systems. We conclude that our measurements indicate that the (double) ridge observed in p-Pb at $\sqrt{s_{\rm NN}} = 5.02$ TeV arises from global azimuthal correlations, rather than from few-particle correlations which decrease with multiplicity. These measurements provide key constraints to the initial state and transport properties in p-Pb and Pb-Pb collisions.

ACKNOWLEDGMENTS

The ALICE Collaboration would like to thank all its engineers and technicians for their invaluable contributions to the construction of the experiment and the CERN accelerator teams for the outstanding performance of the LHC complex. The ALICE Collaboration gratefully acknowledges the resources and support provided by all Grid centres and the Worldwide LHC Computing Grid (WLCG) collaboration. The ALICE Collaboration would like to thank the authors of the theoretical calculations for providing their results. The ALICE Collaboration acknowledges the following funding agencies for their support in building and running the ALICE detector: State Committee of Science, World Federation of Scientists (WFS) and Swiss Fonds Kidagan, Armenia; Conselho Nacional de Desenvolvimento Científico e Tecnológico (CNPq), Financiadora de Estudos e Projetos (FINEP), Fundação de Amparo à Pesquisa do Estado de São Paulo (FAPESP); National Natural Science Foundation of China (NSFC), the Chinese Ministry of Education (CMOE) and the Ministry of Science and Technology of China (MSTC); Ministry of Education and Youth of the Czech Republic; Danish Natural Science Research Council, the Carlsberg Foundation and the Danish National Research Foundation; The European Research Council under the European Community's Seventh Framework Programme; Helsinki Institute of Physics and the Academy of Finland; French CNRS-IN2P3, the 'Region Pays de Loire', 'Region Alsace', 'Region Auvergne' and CEA, France; German BMBF and the Helmholtz Association; General Secretariat for Research and Technology, Ministry of Development, Greece; Hungarian OTKA and National Office for Research and Technology (NKTH); Department of Atomic Energy and Department of Science and Technology of the Government of India; Istituto Nazionale di Fisica Nucleare (INFN) and Centro Fermi - Museo Storico della Fisica e Centro Studi e Ricerche "Enrico Fermi", Italy; MEXT Grant-in-Aid for Specially Promoted Research, Japan; Joint Institute for Nuclear Research, Dubna; National Research Foundation of Korea (NRF); CONACYT, DGAPA, México, ALFA-EC and the EPLANET Program (European Particle Physics Latin American Network); Stichting voor Fundamenteel Onderzoek der Materie (FOM) and the Nederlandse Organisatie voor Wetenschappelijk Onderzoek (NWO), Netherlands; Research

Council of Norway (NFR); Polish Ministry of Science and Higher Education; National Science Centre, Poland; Ministry of National Education/Institute for Atomic Physics and CNCS-UEFISCDI - Romania; Ministry of Education and Science of Russian Federation, Russian Academy of Sciences, Russian Federal Agency of Atomic Energy, Russian Federal Agency for Science and Innovations and The Russian Foundation for Basic Research; Ministry of Education of Slovakia; Department of Science and Technology, South Africa; CIEMAT, EELA, Ministerio de Economía y Competitividad (MINECO) of Spain, Xunta de Galicia (Consellería de Educación), CEADEN, Cubaenergía, Cuba, and IAEA (International Atomic Energy Agency); Swedish Research Council (VR) and Knut & Alice Wallenberg Foundation (KAW); Ukraine Ministry of Education and Science; United Kingdom Science and Technology Facilities Council (STFC); The United States Department of Energy, the United States National Science Foundation, the State of Texas, and the State of Ohio.

APPENDIX

TABLE II. Relation of charged track multiplicity $N_{\rm ch}$ to the fraction of hadronic cross section in p-Pb at $\sqrt{s_{\rm NN}} = 5.02$ TeV collisions. There is a 3.5% uncertainty in the cross section values. $N_{\rm ch}$ corresponds to the number of charged tracks with $0.2 < p_T < 3$ GeV/c and $|\eta| < 1$. The corrected values of $N_{\rm ch}$ have a systematic uncertainty of 6.0%.

Uncorrected $N_{\rm ch}$ bin	Corrected $\langle N_{\rm ch}\rangle$	Fractional of hadronic cross section within bin	Fraction of hadronic cross section above lower bin edge
[6,12]	12.0	0.154	0.826
[12,18]	19.5	0.138	0.673
[18,24]	27.1	0.122	0.535
[24,30]	34.6	0.105	0.412
[30,40]	44.3	0.132	0.308
[40,50]	56.8	0.0836	0.176
[50,60]	69.2	0.0477	0.0921
[60,70]	81.6	0.0245	0.0444
[70,80]	94.1	0.0116	0.0199
[80,100]	110	0.00712	0.00831
[100,120]	135	0.00106	0.00120
[120,140]	159	0.00012	0.00014
[140,180]	186	0.00001	0.00001

TABLE III. Relation of charged track multiplicity $N_{\rm ch}$ to the fraction of hadronic cross section in Pb-Pb at $\sqrt{s_{\rm NN}} = 2.76$ TeV collisions. There is a 1% uncertainty in the cross section values. $N_{\rm ch}$ corresponds to the number of charged tracks with $0.2 < p_T < 3$ GeV/c and $|\eta| < 1$. The corrected values of $N_{\rm ch}$ have a systematic uncertainty of 6.0%.

Uncorrected $N_{\rm ch}$ bin	Corrected $\langle N_{\rm ch}\rangle$	Fraction of hadronic cross section within bin	Fraction of hadronic cross section above lower bin edge
[6,26]	19.82	0.111	0.928
[26,46]	46.7	0.0616	0.817
[46,76]	79.0	0.0615	0.755
[76,106]	118	0.0446	0.694
[106,150]	166	0.0504	0.649
[150,200]	227	0.0453	0.599
[200,250]	292	0.0377	0.553
[250,300]	358	0.0326	0.516
[300,350]	423	0.0289	0.483
[350,400]	488	0.0261	0.454
[400,450]	552	0.0238	0.428
[450,500]	618	0.0221	0.404
[500,600]	714	0.0397	0.382
[600,700]	843	0.0351	0.342
[700,800]	973	0.0316	0.307
[800,900]	1103	0.0286	0.276
[900,1000]	1233	0.0262	0.247

TABLE III. (*Continued.*)

Uncorrected N_{ch} bin	Corrected $\langle N_{\mathrm{ch}} \rangle$	Fraction of hadronic cross section within bin	Fraction of hadronic cross section above lower bin edge
[1000,1200]	1425	0.0466	0.221
[1200,1400]	1684	0.0402	0.174
[1400,1600]	1944	0.0352	0.134
[1600,1800]	2203	0.0307	0.0990
[1800,2000]	2462	0.0268	0.0683
[2000,2400]	2819	0.0388	0.0415
[1900,1950]	2497	0.00656	0.0544
[1950,2000]	2562	0.00635	0.0478
[2000,2050]	2627	0.00617	0.0415
[2050,2100]	2692	0.00594	0.0353
[2100,2150]	2757	0.00570	0.0293
[2150,2200]	2822	0.00544	0.0236
[2200,2250]	2886	0.00502	0.0182
[2250,2300]	2951	0.00445	0.0132
[2300,2350]	3015	0.00353	0.00873
[2350,2400]	3079	0.00249	0.00520
[2400,2450]	3143	0.00151	0.00271
[2450,2500]	3206	0.00074	0.00120
[2500,2550]	3270	0.00031	0.00045
[2550,2600]	3334	0.00010	0.00014

[1] S. Voloshin and Y. Zhang, Z. Phys. C **70**, 665 (1996).
[2] B. Back *et al.*, Nucl. Phys. A **757**, 28 (2005).
[3] I. Arsene *et al.*, Nucl. Phys. A **757**, 1 (2005).
[4] K. Adcox *et al.*, Nucl. Phys. A **757**, 184 (2005).
[5] J. Adams *et al.*, Nucl. Phys. A **757**, 102 (2005).
[6] K. Aamodt *et al.*, Phys. Rev. Lett. **105**, 252302 (2010).
[7] K. Aamodt *et al.*, Phys. Rev. Lett. **107**, 032301 (2011).
[8] K. Aamodt *et al.*, Phys. Lett. B **708**, 249 (2012).
[9] G. Aad *et al.*, Phys. Rev. C **86**, 014907 (2012).
[10] S. Chatrchyan *et al.*, Eur. Phys. J. C **72**, 2012 (2012).
[11] L. Adamczyk *et al.*, Phys. Rev. C **88**, 014904 (2013).
[12] S. Chatrchyan *et al.*, Phys. Lett. B **718**, 795 (2013).
[13] B. Abelev *et al.*, Phys. Lett. B **719**, 29 (2013).
[14] G. Aad *et al.*, Phys. Rev. Lett. **110**, 182302 (2013).
[15] G. Aad *et al.*, Phys. Lett. B **725**, 60 (2013).
[16] S. Chatrchyan *et al.*, Phys. Lett. B **724**, 213 (2013).
[17] B. Abelev *et al.*, Phys. Lett. B **719**, 18 (2013).
[18] B. B. Abelev *et al.*, Phys. Lett. B **728**, 25 (2014).
[19] P. Bozek and W. Broniowski, Phys. Lett. B **718**, 1557 (2013).
[20] K. Dusling and R. Venugopalan, Phys. Rev. D **87**, 054014 (2013).
[21] A. Dumitru, T. Lappi, and L. McLerran, Nucl. Phys. A **922**, 140 (2014).
[22] G. Basar and D. Teaney, Nucl. Phys. A (to be published).
[23] N. Borghini, P. M. Dinh, and J.-Y. Ollitrault, Phys. Rev. C **64**, 054901 (2001).
[24] A. Bilandzic, R. Snellings, and S. Voloshin, Phys. Rev. C **83**, 044913 (2011).
[25] S. A. Voloshin, A. M. Poskanzer, and R. Snellings, in *Landolt-Boernstein, Relativistic Heavy Ion Physics*, Vol. 23 (Springer-Verlag, Berlin, 2010), pp. 293–333.
[26] A. Bilandzic, Ph.D. thesis, Utrecht University, 2011.
[27] K. Aamodt *et al.*, J. Instrum. **3**, S08002 (2008).
[28] B. Abelev *et al.*, J. High Energy Phys. 03 (2012) 053.
[29] X.-N. Wang and M. Gyulassy, Phys. Rev. D **44**, 3501 (1991).
[30] S. Roesler, R. Engel, and J. Ranft, in *Proceedings of the International Conference on Advanced Monte Carlo for Radiation Physics, Particle Transport Simulation and Applications (MC 2000)* (Springer-Verlag, Berlin, 2001), pp. 1033–1038.
[31] R. Brun, F. Carminati, and S. Giani, "GEANT Detector Description and Simulation Tool" (1994).
[32] ALICE technical design report of the computing, CERN-LHCC-2005-018 (2005).
[33] Z.-W. Lin, C. M. Ko, B.-A. Li, B. Zhang, and S. Pal, Phys. Rev. C **72**, 064901 (2005).
[34] G.-L. Ma and A. Bzdak, arXiv:1404.4129.
[35] L. Yan and J.-Y. Ollitrault, Phys. Rev. Lett. **112**, 082301 (2014).
[36] S. A. Voloshin, A. M. Poskanzer, A. Tang, and G. Wang, Phys. Lett. B **659**, 537 (2008).
[37] A. Bzdak, P. Bozek, and L. McLerran, Nucl. Phys. A **927**, 15 (2014).
[38] G. Agakishiev *et al.*, Phys. Rev. C **86**, 014904 (2012).
[39] H. Wang and P. Sorensen, arXiv:1406.7522.
[40] A. R. Timmins, J. Phys.: Conf. Ser. **446**, 012031 (2013).
[41] G. Aad *et al.*, J. High Energy Phys. 11 (2013) 183.
[42] B. Alver *et al.*, Phys. Rev. C **81**, 034915 (2010).
[43] W. Broniowski, P. Bozek, and M. Rybczynski, Phys. Rev. C **76**, 054905 (2007).

B. Abelev,[1] J. Adam,[2] D. Adamová,[3] M. M. Aggarwal,[4] G. Aglieri Rinella,[5] M. Agnello,[6,7] A. Agostinelli,[8] N. Agrawal,[9] Z. Ahammed,[10] N. Ahmad,[11] I. Ahmed,[12] S. U. Ahn,[13] S. A. Ahn,[13] I. Aimo,[6,7] S. Aiola,[14] M. Ajaz,[12] A. Akindinov,[15] S. N. Alam,[10] D. Aleksandrov,[16] B. Alessandro,[6] D. Alexandre,[17] A. Alici,[18,19] A. Alkin,[20] J. Alme,[21] T. Alt,[22] S. Altinpinar,[23] I. Altsybeev,[24] C. Alves Garcia Prado,[25] C. Andrei,[26] A. Andronic,[27] V. Anguelov,[28] J. Anielski,[29] T. Antičić,[30] F. Antinori,[31] P. Antonioli,[19] L. Aphecetche,[32] H. Appelshäuser,[33] S. Arcelli,[8] N. Armesto,[34] R. Arnaldi,[6] T. Aronsson,[14] I. C. Arsene,[27,35] M. Arslandok,[33] A. Augustinus,[5] R. Averbeck,[27] T. C. Awes,[36] M. D. Azmi,[11,37] M. Bach,[22] A. Badalà,[38] Y. W. Baek,[39,40] S. Bagnasco,[6] R. Bailhache,[33] R. Bala,[41] A. Baldisseri,[42] F. Baltasar Dos Santos Pedrosa,[5] R. C. Baral,[43] R. Barbera,[44] F. Barile,[45] G. G. Barnaföldi,[46] L. S. Barnby,[17] V. Barret,[40] J. Bartke,[47] M. Basile,[8] N. Bastid,[40] S. Basu,[10] B. Bathen,[29] G. Batigne,[32] A. Batista Camejo,[40] B. Batyunya,[48] P. C. Batzing,[35] C. Baumann,[33] I. G. Bearden,[49] H. Beck,[33] C. Bedda,[7] N. K. Behera,[9] I. Belikov,[50] F. Bellini,[8] R. Bellwied,[51] E. Belmont-Moreno,[52] R. Belmont III,[53] V. Belyaev,[54] G. Bencedi,[46] S. Beole,[55] I. Berceanu,[26] A. Bercuci,[26] Y. Berdnikov,[56,57] D. Berenyi,[46] M. E. Berger,[58] R. A. Bertens,[59] D. Berzano,[55] L. Betev,[5] A. Bhasin,[41] I. R. Bhat,[41] A. K. Bhati,[4] B. Bhattacharjee,[60] J. Bhom,[61] L. Bianchi,[55] N. Bianchi,[62] C. Bianchin,[59] J. Bielčík,[2] J. Bielčíková,[3] A. Bilandzic,[49] S. Bjelogrlic,[59] F. Blanco,[63] D. Blau,[16] C. Blume,[33] F. Bock,[64,28] A. Bogdanov,[54] H. Bøggild,[49] M. Bogolyubsky,[65] F. V. Böhmer,[58] L. Boldizsár,[46] M. Bombara,[66] J. Book,[33] H. Borel,[42] A. Borissov,[53,67] F. Bossú,[68] M. Botje,[69] E. Botta,[55] S. Böttger,[70] P. Braun-Munzinger,[27] M. Bregant,[25] T. Breitner,[70] T. A. Broker,[33] T. A. Browning,[71] M. Broz,[2] E. Bruna,[6] G. E. Bruno,[45] D. Budnikov,[72] H. Buesching,[33] S. Bufalino,[6] P. Buncic,[5] O. Busch,[28] Z. Buthelezi,[68] D. Caffarri,[5,73] X. Cai,[74] H. Caines,[14] L. Calero Diaz,[62] A. Caliva,[59] E. Calvo Villar,[75] P. Camerini,[76] F. Carena,[5] W. Carena,[5] J. Castillo Castellanos,[42] E. A. R. Casula,[77] V. Catanescu,[26] C. Cavicchioli,[5] C. Ceballos Sanchez,[78] J. Cepila,[2] P. Cerello,[6] B. Chang,[79] S. Chapeland,[5] J. L. Charvet,[42] S. Chattopadhyay,[10] S. Chattopadhyay,[80] V. Chelnokov,[20] M. Cherney,[81] C. Cheshkov,[82] B. Cheynis,[82] V. Chibante Barroso,[5] D. D. Chinellato,[83,51] P. Chochula,[5] M. Chojnacki,[49] S. Choudhury,[10] P. Christakoglou,[69] C. H. Christensen,[49] P. Christiansen,[84] T. Chujo,[61] S. U. Chung,[67] C. Cicalo,[85] L. Cifarelli,[8,18] F. Cindolo,[19] J. Cleymans,[37] F. Colamaria,[45] D. Colella,[45] A. Collu,[77] M. Colocci,[8] G. Conesa Balbastre,[86] Z. Conesa del Valle,[87] M. E. Connors,[14] J. G. Contreras,[88,2] T. M. Cormier,[36,53] Y. Corrales Morales,[55] P. Cortese,[89] I. Cortés Maldonado,[90] M. R. Cosentino,[25] F. Costa,[5] P. Crochet,[40] R. Cruz Albino,[88] E. Cuautle,[91] L. Cunqueiro,[62,5] A. Dainese,[31] R. Dang,[74] A. Danu,[92] D. Das,[80] I. Das,[87] K. Das,[80] S. Das,[93] A. Dash,[83] S. Dash,[9] S. De,[10] H. Delagrange,[32,*] A. Deloff,[94] E. Dénes,[46] G. D'Erasmo,[45] A. De Caro,[95,18] G. de Cataldo,[96] J. de Cuveland,[22] A. De Falco,[77] D. De Gruttola,[95,18] N. De Marco,[6] S. De Pasquale,[95] R. de Rooij,[59] M. A. Diaz Corchero,[63] T. Dietel,[29,37] P. Dillenseger,[33] R. Divià,[5] D. Di Bari,[45] S. Di Liberto,[97] A. Di Mauro,[5] P. Di Nezza,[62] Ø. Djuvsland,[23] A. Dobrin,[59] T. Dobrowolski,[94] D. Domenicis Gimenez,[25] B. Dönigus,[33] O. Dordic,[35] S. Dørheim,[58] A. K. Dubey,[10] A. Dubla,[59] L. Ducroux,[82] P. Dupieux,[40] A. K. Dutta Majumdar,[80] T. E. Hilden,[98] R. J. Ehlers,[14] D. Elia,[96] H. Engel,[70] B. Erazmus,[5,32] H. A. Erdal,[21] D. Eschweiler,[22] B. Espagnon,[87] M. Esposito,[5] M. Estienne,[32] S. Esumi,[61] D. Evans,[17] S. Evdokimov,[65] D. Fabris,[31] J. Faivre,[86] D. Falchieri,[8] A. Fantoni,[62] M. Fasel,[28,64] D. Fehlker,[23] L. Feldkamp,[29] D. Felea,[92] A. Feliciello,[6] G. Feofilov,[24] J. Ferencei,[3] A. Fernández Téllez,[90] E. G. Ferreiro,[34] A. Ferretti,[55] A. Festanti,[73] J. Figiel,[47] M. A. S. Figueredo,[99] S. Filchagin,[72] D. Finogeev,[100] F. M. Fionda,[45] E. M. Fiore,[45] E. Floratos,[101] M. Floris,[5] S. Foertsch,[68] P. Foka,[27] S. Fokin,[16] E. Fragiacomo,[102] A. Francescon,[5,73] U. Frankenfeld,[27] U. Fuchs,[5] C. Furget,[86] A. Furs,[100] M. Fusco Girard,[95] J. J. Gaardhøje,[49] M. Gagliardi,[55] A. M. Gago,[75] M. Gallio,[55] D. R. Gangadharan,[103,64] P. Ganoti,[36,101] C. Garabatos,[27] E. Garcia-Solis,[104] C. Gargiulo,[5] I. Garishvili,[1] J. Gerhard,[22] M. Germain,[32] A. Gheata,[5] M. Gheata,[5,92] B. Ghidini,[45] P. Ghosh,[10] S. K. Ghosh,[93] P. Gianotti,[62] P. Giubellino,[5] E. Gladysz-Dziadus,[47] P. Glässel,[28] A. Gomez Ramirez,[70] P. González-Zamora,[63] S. Gorbunov,[22] L. Görlich,[47] S. Gotovac,[105] L. K. Graczykowski,[106] A. Grelli,[59] A. Grigoras,[5] C. Grigoras,[5] V. Grigoriev,[54] A. Grigoryan,[107] S. Grigoryan,[48] B. Grinyov,[20] N. Grion,[102] J. F. Grosse-Oetringhaus,[5] J.-Y. Grossiord,[82] R. Grosso,[5] F. Guber,[100] R. Guernane,[86] B. Guerzoni,[8] M. Guilbaud,[82] K. Gulbrandsen,[49] H. Gulkanyan,[107] M. Gumbo,[37] T. Gunji,[108] A. Gupta,[41] R. Gupta,[41] K. H. Khan,[12] R. Haake,[29] Ø. Haaland,[23] C. Hadjidakis,[87] M. Haiduc,[92] H. Hamagaki,[108] G. Hamar,[46] L. D. Hanratty,[17] A. Hansen,[49] J. W. Harris,[14] H. Hartmann,[22] A. Harton,[104] D. Hatzifotiadou,[19] S. Hayashi,[108] S. T. Heckel,[33] M. Heide,[29] H. Helstrup,[21] A. Herghelegiu,[26] G. Herrera Corral,[88] B. A. Hess,[109] K. F. Hetland,[21] B. Hippolyte,[50] J. Hladky,[110] P. Hristov,[5] M. Huang,[23] T. J. Humanic,[103] N. Hussain,[60] D. Hutter,[22] D. S. Hwang,[111] R. Ilkaev,[72] I. Ilkiv,[94] M. Inaba,[61] G. M. Innocenti,[55] C. Ionita,[5] M. Ippolitov,[16] M. Irfan,[11] M. Ivanov,[27] V. Ivanov,[57] A. Jachołkowski,[44] P. M. Jacobs,[64] C. Jahnke,[25] H. J. Jang,[13] M. A. Janik,[106] P. H. S. Y. Jayarathna,[51] C. Jena,[73] S. Jena,[51] R. T. Jimenez Bustamante,[91] P. G. Jones,[17] H. Jung,[39] A. Jusko,[17] V. Kadyshevskiy,[48] S. Kalcher,[22] P. Kalinak,[112] A. Kalweit,[5] J. Kamin,[33] J. H. Kang,[113] V. Kaplin,[54] S. Kar,[10] A. Karasu Uysal,[114] O. Karavichev,[100] T. Karavicheva,[100] E. Karpechev,[100] U. Kebschull,[70] R. Keidel,[115] D. L. D. Keijdener,[59] M. Keil SVN,[5] M. M. Khan,[116,11] P. Khan,[80] S. A. Khan,[10] A. Khanzadeev,[57] Y. Kharlov,[65] B. Kileng,[21] B. Kim,[113] D. W. Kim,[13,39] D. J. Kim,[79] J. S. Kim,[39] M. Kim,[39] M. Kim,[113] S. Kim,[111] T. Kim,[113] S. Kirsch,[22] I. Kisel,[22] S. Kiselev,[15] A. Kisiel,[106] G. Kiss,[46] J. L. Klay,[117] J. Klein,[28] C. Klein-Bösing,[29] A. Kluge,[5] M. L. Knichel,[27] A. G. Knospe,[118] C. Kobdaj,[119,5] M. Kofarago,[5] M. K. Köhler,[27] T. Kollegger,[22] A. Kolojvari,[24] V. Kondratiev,[24] N. Kondratyeva,[54] A. Konevskikh,[100] V. Kovalenko,[24] M. Kowalski,[47] S. Kox,[86] G. Koyithatta Meethaleveedu,[9] J. Kral,[79] I. Králik,[112] A. Kravčáková,[66] M. Krelina,[2] M. Kretz,[22] M. Krivda,[17,112] F. Krizek,[3] E. Kryshen,[5] M. Krzewicki,[27,22] V. Kučera,[3] Y. Kucheriaev,[16,*] T. Kugathasan,[5] C. Kuhn,[50] P. G. Kuijer,[69] I. Kulakov,[33] J. Kumar,[9] P. Kurashvili,[94] A. Kurepin,[100] A. B. Kurepin,[100] A. Kuryakin,[72] S. Kushpil,[3] M. J. Kweon,[120,28] Y. Kwon,[113] P. Ladron de Guevara,[91] C. Lagana Fernandes,[25] I. Lakomov,[87] R. Langoy,[121] C. Lara,[70] A. Lardeux,[32] A. Lattuca,[55] S. L. La Pointe,[59,6] P. La Rocca,[44] R. Lea,[76] L. Leardini,[28]

G. R. Lee,[17] I. Legrand,[5] J. Lehnert,[33] R. C. Lemmon,[122] V. Lenti,[96] E. Leogrande,[59] M. Leoncino,[55] I. León Monzón,[123] P. Lévai,[46] S. Li,[74,40] J. Lien,[121] R. Lietava,[17] S. Lindal,[35] V. Lindenstruth,[22] C. Lippmann,[27] M. A. Lisa,[103] H. M. Ljunggren,[84] D. F. Lodato,[59] P. I. Loenne,[23] V. R. Loggins,[53] V. Loginov,[54] D. Lohner,[28] C. Loizides,[64] X. Lopez,[40] E. López Torres,[78] X.-G. Lu,[28] P. Luettig,[33] M. Lunardon,[73] G. Luparello,[59,76] R. Ma,[14] A. Maevskaya,[100] M. Mager,[5] D. P. Mahapatra,[43] S. M. Mahmood,[35] A. Maire,[28,50] R. D. Majka,[14] M. Malaev,[57] I. Maldonado Cervantes,[91] L. Malinina,[124,48] D. Mal'Kevich,[15] P. Malzacher,[27] A. Mamonov,[72] L. Manceau,[6] V. Manko,[16] F. Manso,[40] V. Manzari,[96] M. Marchisone,[40,55] J. Mareš,[110] G. V. Margagliotti,[76] A. Margotti,[19] A. Marín,[27] C. Markert,[118] M. Marquard,[33] I. Martashvili,[125] N. A. Martin,[27] P. Martinengo,[5] M. I. Martínez,[90] G. Martínez García,[32] J. Martin Blanco,[32] Y. Martynov,[20] A. Mas,[32] S. Masciocchi,[27] M. Masera,[55] A. Masoni,[85] L. Massacrier,[32] A. Mastroserio,[45] A. Matyja,[47] C. Mayer,[47] J. Mazer,[125] M. A. Mazzoni,[97] F. Meddi,[126] A. Menchaca-Rocha,[52] E. Meninno,[95] J. Mercado Pérez,[28] M. Meres,[127] Y. Miake,[61] K. Mikhaylov,[48,15] L. Milano,[5] J. Milosevic,[128,35] A. Mischke,[59] A. N. Mishra,[129] D. Miśkowiec,[27] J. Mitra,[10] C. M. Mitu,[92] J. Mlynarz,[53] N. Mohammadi,[59] B. Mohanty,[130,10] L. Molnar,[50] L. Montaño Zetina,[88] E. Montes,[63] M. Morando,[73] D. A. Moreira De Godoy,[25] S. Moretto,[73] A. Morreale,[32] A. Morsch,[5] V. Muccifora,[62] E. Mudnic,[105] D. Mühlheim,[29] S. Muhuri,[10] M. Mukherjee,[10] H. Müller,[5] M. G. Munhoz,[25] S. Murray,[37] L. Musa,[5] J. Musinsky,[112] B. K. Nandi,[9] R. Nania,[19] E. Nappi,[96] C. Nattrass,[125] K. Nayak,[130] T. K. Nayak,[10] S. Nazarenko,[72] A. Nedosekin,[15] M. Nicassio,[27] M. Niculescu,[5,92] B. S. Nielsen,[49] S. Nikolaev,[16] S. Nikulin,[16] V. Nikulin,[57] B. S. Nilsen,[81] F. Noferini,[18,19] P. Nomokonov,[48] G. Nooren,[59] J. Norman,[99] A. Nyanin,[16] J. Nystrand,[23] H. Oeschler,[28] S. Oh,[14] S. K. Oh,[131,39,†] A. Okatan,[114] L. Olah,[46] J. Oleniacz,[106] A. C. Oliveira Da Silva,[25] J. Onderwaater,[27] C. Oppedisano,[6] A. Ortiz Velasquez,[91,84] A. Oskarsson,[84] J. Otwinowski,[47,27] K. Oyama,[28] M. Ozdemir,[33] P. Sahoo,[129] Y. Pachmayer,[28] M. Pachr,[2] P. Pagano,[95] G. Paić,[91] F. Painke,[22] C. Pajares,[34] S. K. Pal,[10] A. Palmeri,[38] D. Pant,[9] V. Papikyan,[107] G. S. Pappalardo,[38] P. Pareek,[129] W. J. Park,[27] S. Parmar,[4] A. Passfeld,[29] D. I. Patalakha,[65] V. Paticchio,[96] B. Paul,[80] T. Pawlak,[106] T. Peitzmann,[59] H. Pereira Da Costa,[42] E. Pereira De Oliveira Filho,[25] D. Peresunko,[16] C. E. Pérez Lara,[69] A. Pesci,[19] V. Peskov,[33] Y. Pestov,[132] V. Petráček,[2] M. Petran,[2] M. Petris,[26] M. Petrovici,[26] C. Petta,[44] S. Piano,[102] M. Pikna,[127] P. Pillot,[32] O. Pinazza,[19,5] L. Pinsky,[51] D. B. Piyarathna,[51] M. Płoskoń,[64] M. Planinic,[133,30] J. Pluta,[106] S. Pochybova,[46] P. L. M. Podesta-Lerma,[123] M. G. Poghosyan,[81,5] E. H. O. Pohjoisaho,[98] B. Polichtchouk,[65] N. Poljak,[30,133] A. Pop,[26] S. Porteboeuf-Houssais,[40] J. Porter,[64] B. Potukuchi,[41] S. K. Prasad,[53,93] R. Preghenella,[19,18] F. Prino,[6] C. A. Pruneau,[53] I. Pshenichnov,[100] G. Puddu,[77] P. Pujahari,[53] V. Punin,[72] J. Putschke,[53] H. Qvigstad,[35] A. Rachevski,[102] S. Raha,[93] J. Rak,[79] A. Rakotozafindrabe,[42] L. Ramello,[89] R. Raniwala,[134] S. Raniwala,[134] S. S. Räsänen,[98] B. T. Rascanu,[33] D. Rathee,[4] A. W. Rauf,[12] V. Razazi,[77] K. F. Read,[125] J. S. Real,[86] K. Redlich,[135,94] R. J. Reed,[53,14] A. Rehman,[23] P. Reichelt,[33] M. Reicher,[59] F. Reidt,[28,5] R. Renfordt,[33] A. R. Reolon,[62] A. Reshetin,[100] F. Rettig,[22] J.-P. Revol,[5] K. Reygers,[28] V. Riabov,[57] R. A. Ricci,[136] T. Richert,[84] M. Richter,[35] P. Riedler,[5] W. Riegler,[5] F. Riggi,[44] A. Rivetti,[6] E. Rocco,[59] M. Rodríguez Cahuantzi,[90] A. Rodriguez Manso,[69] K. Røed,[35] E. Rogochaya,[48] S. Rohni,[41] D. Rohr,[22] D. Röhrich,[23] R. Romita,[122,99] F. Ronchetti,[62] L. Ronflette,[32] P. Rosnet,[40] A. Rossi,[5] F. Roukoutakis,[101] A. Roy,[129] C. Roy,[50] P. Roy,[80] A. J. Rubio Montero,[63] R. Rui,[76] R. Russo,[55] E. Ryabinkin,[16] Y. Ryabov,[57] A. Rybicki,[47] S. Sadovsky,[65] K. Šafařík,[5] B. Sahlmuller,[33] R. Sahoo,[129] P. K. Sahu,[43] J. Saini,[10] S. Sakai,[62] C. A. Salgado,[34] J. Salzwedel,[103] S. Sambyal,[41] V. Samsonov,[57] X. Sanchez Castro,[50] F. J. Sánchez Rodríguez,[123] L. Šándor,[112] A. Sandoval,[52] M. Sano,[61] G. Santagati,[44] D. Sarkar,[10] E. Scapparone,[19] F. Scarlassara,[73] R. P. Scharenberg,[71] C. Schiaua,[26] R. Schicker,[28] C. Schmidt,[27] H. R. Schmidt,[109] S. Schuchmann,[33] J. Schukraft,[5] M. Schulc,[2] T. Schuster,[14] Y. Schutz,[32,5] K. Schwarz,[27] K. Schweda,[27] G. Scioli,[8] E. Scomparin,[6] R. Scott,[125] G. Segato,[73] J. E. Seger,[81] Y. Sekiguchi,[108] I. Selyuzhenkov,[27] J. Seo,[67] E. Serradilla,[63,52] A. Sevcenco,[92] A. Shabetai,[32] G. Shabratova,[48] R. Shahoyan,[5] A. Shangaraev,[65] N. Sharma,[125] S. Sharma,[41] K. Shigaki,[137] K. Shtejer,[55] Y. Sibiriak,[16] S. Siddhanta,[85] T. Siemiarczuk,[94] D. Silvermyr,[36] C. Silvestre,[86] G. Simatovic,[133] R. Singaraju,[10] R. Singh,[41] S. Singha,[10,130] V. Singhal,[10] B. C. Sinha,[10] T. Sinha,[80] B. Sitar,[127] M. Sitta,[89] T. B. Skaali,[35] K. Skjerdal,[23] M. Slupecki,[79] N. Smirnov,[14] R. J. M. Snellings,[59] C. Søgaard,[84] R. Soltz,[1] J. Song,[67] M. Song,[113] F. Soramel,[73] S. Sorensen,[125] M. Spacek,[2] E. Spiriti,[62] I. Sputowska,[47] M. Spyropoulou-Stassinaki,[101] B. K. Srivastava,[71] J. Stachel,[28] I. Stan,[92] G. Stefanek,[94] M. Steinpreis,[103] E. Stenlund,[84] G. Steyn,[68] J. H. Stiller,[28] D. Stocco,[32] M. Stolpovskiy,[65] P. Strmen,[127] A. A. P. Suaide,[25] T. Sugitate,[137] C. Suire,[87] M. Suleymanov,[12] R. Sultanov,[15] M. Šumbera,[3] T. Susa,[30] T. J. M. Symons,[64] A. Szabo,[127] A. Szanto de Toledo,[25] I. Szarka,[127] A. Szczepankiewicz,[5] M. Szymanski,[106] J. Takahashi,[83] M. A. Tangaro,[45] J. D. Tapia Takaki,[138,87] A. Tarantola Peloni,[33] A. Tarazona Martinez,[5] M. G. Tarzila,[26] A. Tauro,[5] G. Tejeda Muñoz,[90] A. Telesca,[5] C. Terrevoli,[77] J. Thäder,[27] D. Thomas,[59] R. Tieulent,[82] A. R. Timmins,[51] A. Toia,[33,31] V. Trubnikov,[20] W. H. Trzaska,[79] T. Tsuji,[108] A. Tumkin,[72] R. Turrisi,[31] T. S. Tveter,[35] K. Ullaland,[23] A. Uras,[82] G. L. Usai,[77] M. Vajzer,[3] M. Vala,[112,48] L. Valencia Palomo,[40] S. Vallero,[55,28] P. Vande Vyvre,[5] J. Van Der Maarel,[59] J. W. Van Hoorne,[5] M. van Leeuwen,[59] A. Vargas,[90] M. Vargyas,[79] R. Varma,[9] M. Vasileiou,[101] A. Vasiliev,[16] V. Vechernin,[24] M. Veldhoen,[59] A. Velure,[23] M. Venaruzzo,[76,136] E. Vercellin,[55] S. Vergara Limón,[90] R. Vernet,[139] M. Verweij,[53] L. Vickovic,[105] G. Viesti,[73] J. Viinikainen,[79] Z. Vilakazi,[68] O. Villalobos Baillie,[17] A. Vinogradov,[16] L. Vinogradov,[24] Y. Vinogradov,[72] T. Virgili,[95] Y. P. Viyogi,[10] A. Vodopyanov,[48] M. A. Völkl,[28] K. Voloshin,[15] S. A. Voloshin,[53] G. Volpe,[5] B. von Haller,[5] I. Vorobyev,[24] D. Vranic,[27,5] J. Vrláková,[66] B. Vulpescu,[40] A. Vyushin,[72] B. Wagner,[23] J. Wagner,[27] V. Wagner,[2] M. Wang,[74,32] Y. Wang,[28] D. Watanabe,[61] M. Weber,[5,51] J. P. Wessels,[29] U. Westerhoff,[29] J. Wiechula,[109] J. Wikne,[35] M. Wilde,[29] G. Wilk,[94] J. Wilkinson,[28] M. C. S. Williams,[19] B. Windelband,[28] M. Winn,[28] C. G. Yaldo,[53] Y. Yamaguchi,[108] H. Yang,[59] P. Yang,[74] S. Yang,[23] S. Yano,[137] S. Yasnopolskiy,[16] J. Yi,[67] Z. Yin,[74] I.-K. Yoo,[67] I. Yushmanov,[16] V. Zaccolo,[49] C. Zach,[2] A. Zaman,[12]

C. Zampolli,[19] S. Zaporozhets,[48] A. Zarochentsev,[24] P. Závada,[110] N. Zaviyalov,[72] H. Zbroszczyk,[106] I. S. Zgura,[92] M. Zhalov,[57] H. Zhang,[74] X. Zhang,[74,64] Y. Zhang,[74] C. Zhao,[35] N. Zhigareva,[15] D. Zhou,[74] F. Zhou,[74] Y. Zhou,[59] Zhuo Zhou,[23] H. Zhu,[74] J. Zhu,[74] X. Zhu,[74] A. Zichichi,[18,8] A. Zimmermann,[28] M. B. Zimmermann,[29,5] G. Zinovjev,[20] Y. Zoccarato,[82] and M. Zyzak[33]

(ALICE Collaboration)

[1]*Lawrence Livermore National Laboratory, Livermore, California, USA*
[2]*Faculty of Nuclear Sciences and Physical Engineering, Czech Technical University in Prague, Prague, Czech Republic*
[3]*Nuclear Physics Institute, Academy of Sciences of the Czech Republic, Řež u Prahy, Czech Republic*
[4]*Physics Department, Panjab University, Chandigarh, India*
[5]*European Organization for Nuclear Research (CERN), Geneva, Switzerland*
[6]*Sezione INFN, Turin, Italy*
[7]*Politecnico di Torino, Turin, Italy*
[8]*Dipartimento di Fisica e Astronomia dell'Università and Sezione INFN, Bologna, Italy*
[9]*Indian Institute of Technology Bombay (IIT), Mumbai, India*
[10]*Variable Energy Cyclotron Centre, Kolkata, India*
[11]*Department of Physics, Aligarh Muslim University, Aligarh, India*
[12]*COMSATS Institute of Information Technology (CIIT), Islamabad, Pakistan*
[13]*Korea Institute of Science and Technology Information, Daejeon, South Korea*
[14]*Yale University, New Haven, Connecticut, USA*
[15]*Institute for Theoretical and Experimental Physics, Moscow, Russia*
[16]*Russian Research Centre Kurchatov Institute, Moscow, Russia*
[17]*School of Physics and Astronomy, University of Birmingham, Birmingham, United Kingdom*
[18]*Centro Fermi - Museo Storico della Fisica e Centro Studi e Ricerche "Enrico Fermi", Rome, Italy*
[19]*Sezione INFN, Bologna, Italy*
[20]*Bogolyubov Institute for Theoretical Physics, Kiev, Ukraine*
[21]*Faculty of Engineering, Bergen University College, Bergen, Norway*
[22]*Frankfurt Institute for Advanced Studies, Johann Wolfgang Goethe-Universität Frankfurt, Frankfurt, Germany*
[23]*Department of Physics and Technology, University of Bergen, Bergen, Norway*
[24]*V. Fock Institute for Physics, St. Petersburg State University, St. Petersburg, Russia*
[25]*Universidade de São Paulo (USP), São Paulo, Brazil*
[26]*National Institute for Physics and Nuclear Engineering, Bucharest, Romania*
[27]*Research Division and ExtreMe Matter Institute EMMI, GSI Helmholtzzentrum für Schwerionenforschung, Darmstadt, Germany*
[28]*Physikalisches Institut, Ruprecht-Karls-Universität Heidelberg, Heidelberg, Germany*
[29]*Institut für Kernphysik, Westfälische Wilhelms-Universität Münster, Münster, Germany*
[30]*Rudjer Bošković Institute, Zagreb, Croatia*
[31]*Sezione INFN, Padova, Italy*
[32]*SUBATECH, Ecole des Mines de Nantes, Université de Nantes, CNRS-IN2P3, Nantes, France*
[33]*Institut für Kernphysik, Johann Wolfgang Goethe-Universität Frankfurt, Frankfurt, Germany*
[34]*Departamento de Física de Partículas and IGFAE, Universidad de Santiago de Compostela, Santiago de Compostela, Spain*
[35]*Department of Physics, University of Oslo, Oslo, Norway*
[36]*Oak Ridge National Laboratory, Oak Ridge, Tennessee, USA*
[37]*Physics Department, University of Cape Town, Cape Town, South Africa*
[38]*Sezione INFN, Catania, Italy*
[39]*Gangneung-Wonju National University, Gangneung, South Korea*
[40]*Laboratoire de Physique Corpusculaire (LPC), Clermont Université, Université Blaise Pascal, CNRS–IN2P3, Clermont-Ferrand, France*
[41]*Physics Department, University of Jammu, Jammu, India*
[42]*Commissariat à l'Energie Atomique, IRFU, Saclay, France*
[43]*Institute of Physics, Bhubaneswar, India*
[44]*Dipartimento di Fisica e Astronomia dell'Università and Sezione INFN, Catania, Italy*
[45]*Dipartimento Interateneo di Fisica "M. Merlin" and Sezione INFN, Bari, Italy*
[46]*Wigner Research Centre for Physics, Hungarian Academy of Sciences, Budapest, Hungary*
[47]*The Henryk Niewodniczanski Institute of Nuclear Physics, Polish Academy of Sciences, Cracow, Poland*
[48]*Joint Institute for Nuclear Research (JINR), Dubna, Russia*
[49]*Niels Bohr Institute, University of Copenhagen, Copenhagen, Denmark*
[50]*Institut Pluridisciplinaire Hubert Curien (IPHC), Université de Strasbourg, CNRS-IN2P3, Strasbourg, France*
[51]*University of Houston, Houston, Texas, USA*
[52]*Instituto de Física, Universidad Nacional Autónoma de México, Mexico City, Mexico*

[53]*Wayne State University, Detroit, Michigan, USA*
[54]*Moscow Engineering Physics Institute, Moscow, Russia*
[55]*Dipartimento di Fisica dell'Università and Sezione INFN, Turin, Italy*
[56]*St. Petersburg State Polytechnical University, St. Petersburg, Russia*
[57]*Petersburg Nuclear Physics Institute, Gatchina, Russia*
[58]*Physik Department, Technische Universität München, Munich, Germany*
[59]*Institute for Subatomic Physics of Utrecht University, Utrecht, Netherlands*
[60]*Gauhati University, Department of Physics, Guwahati, India*
[61]*University of Tsukuba, Tsukuba, Japan*
[62]*Laboratori Nazionali di Frascati, INFN, Frascati, Italy*
[63]*Centro de Investigaciones Energéticas Medioambientales y Tecnológicas (CIEMAT), Madrid, Spain*
[64]*Lawrence Berkeley National Laboratory, Berkeley, California, USA*
[65]*SSC IHEP of NRC Kurchatov institute, Protvino, Russia*
[66]*Faculty of Science, P.J. Šafárik University, Košice, Slovakia*
[67]*Pusan National University, Pusan, South Korea*
[68]*iThemba LABS, National Research Foundation, Somerset West, South Africa*
[69]*Nikhef, National Institute for Subatomic Physics, Amsterdam, Netherlands*
[70]*Institut für Informatik, Johann Wolfgang Goethe-Universität Frankfurt, Frankfurt, Germany*
[71]*Purdue University, West Lafayette, Indiana, USA*
[72]*Russian Federal Nuclear Center (VNIIEF), Sarov, Russia*
[73]*Dipartimento di Fisica e Astronomia dell'Università and Sezione INFN, Padova, Italy*
[74]*Central China Normal University, Wuhan, China*
[75]*Sección Física, Departamento de Ciencias, Pontificia Universidad Católica del Perú, Lima, Peru*
[76]*Dipartimento di Fisica dell'Università and Sezione INFN, Trieste, Italy*
[77]*Dipartimento di Fisica dell'Università and Sezione INFN, Cagliari, Italy*
[78]*Centro de Aplicaciones Tecnológicas y Desarrollo Nuclear (CEADEN), Havana, Cuba*
[79]*University of Jyväskylä, Jyväskylä, Finland*
[80]*Saha Institute of Nuclear Physics, Kolkata, India*
[81]*Physics Department, Creighton University, Omaha, Nebraska, USA*
[82]*Université de Lyon, Université Lyon 1, CNRS/IN2P3, IPN-Lyon, Villeurbanne, France*
[83]*Universidade Estadual de Campinas (UNICAMP), Campinas, Brazil*
[84]*Division of Experimental High Energy Physics, University of Lund, Lund, Sweden*
[85]*Sezione INFN, Cagliari, Italy*
[86]*Laboratoire de Physique Subatomique et de Cosmologie, Université Grenoble-Alpes, CNRS-IN2P3, Grenoble, France*
[87]*Institut de Physique Nucléaire d'Orsay (IPNO), Université Paris-Sud, CNRS-IN2P3, Orsay, France*
[88]*Centro de Investigación y de Estudios Avanzados (CINVESTAV), Mexico City and Mérida, Mexico*
[89]*Dipartimento di Scienze e Innovazione Tecnologica dell'Università del Piemonte Orientale and Gruppo Collegato INFN, Alessandria, Italy*
[90]*Benemérita Universidad Autónoma de Puebla, Puebla, Mexico*
[91]*Instituto de Ciencias Nucleares, Universidad Nacional Autónoma de México, Mexico City, Mexico*
[92]*Institute of Space Science (ISS), Bucharest, Romania*
[93]*Bose Institute, Department of Physics and Centre for Astroparticle Physics and Space Science (CAPSS), Kolkata, India*
[94]*National Centre for Nuclear Studies, Warsaw, Poland*
[95]*Dipartimento di Fisica "E.R. Caianiello" dell'Università and Gruppo Collegato INFN, Salerno, Italy*
[96]*Sezione INFN, Bari, Italy*
[97]*Sezione INFN, Rome, Italy*
[98]*Helsinki Institute of Physics (HIP), Helsinki, Finland*
[99]*University of Liverpool, Liverpool, United Kingdom*
[100]*Institute for Nuclear Research, Academy of Sciences, Moscow, Russia*
[101]*Physics Department, University of Athens, Athens, Greece*
[102]*Sezione INFN, Trieste, Italy*
[103]*Department of Physics, Ohio State University, Columbus, Ohio, USA*
[104]*Chicago State University, Chicago, Illinois, USA*
[105]*Technical University of Split FESB, Split, Croatia*
[106]*Warsaw University of Technology, Warsaw, Poland*
[107]*A.I. Alikhanyan National Science Laboratory (Yerevan Physics Institute) Foundation, Yerevan, Armenia*
[108]*University of Tokyo, Tokyo, Japan*
[109]*Eberhard Karls Universität Tübingen, Tübingen, Germany*
[110]*Institute of Physics, Academy of Sciences of the Czech Republic, Prague, Czech Republic*
[111]*Department of Physics, Sejong University, Seoul, South Korea*

[112] *Institute of Experimental Physics, Slovak Academy of Sciences, Košice, Slovakia*
[113] *Yonsei University, Seoul, South Korea*
[114] *KTO Karatay University, Konya, Turkey*
[115] *Zentrum für Technologietransfer und Telekommunikation (ZTT), Fachhochschule Worms, Worms, Germany*
[116] *Department of Applied Physics, Aligarh Muslim University, Aligarh, India*
[117] *California Polytechnic State University, San Luis Obispo, California, USA*
[118] *The University of Texas at Austin, Physics Department, Austin, Texas, USA*
[119] *Suranaree University of Technology, Nakhon Ratchasima, Thailand*
[120] *Inha University, Incheon, South Korea*
[121] *Vestfold University College, Tonsberg, Norway*
[122] *Nuclear Physics Group, STFC Daresbury Laboratory, Daresbury, United Kingdom*
[123] *Universidad Autónoma de Sinaloa, Culiacán, Mexico*
[124] *M.V. Lomonosov Moscow State University, D.V. Skobeltsyn Institute of Nuclear Physics, Moscow, Russia*
[125] *University of Tennessee, Knoxville, Tennessee, USA*
[126] *Dipartimento di Fisica dell'Università "La Sapienza" and Sezione INFN Rome, Italy*
[127] *Faculty of Mathematics, Physics and Informatics, Comenius University, Bratislava, Slovakia*
[128] *University of Belgrade, Faculty of Physics and "Vinča" Institute of Nuclear Sciences, Belgrade, Serbia*
[129] *Indian Institute of Technology Indore, Indore (IITI), India*
[130] *National Institute of Science Education and Research, Bhubaneswar, India*
[131] *Konkuk University, Seoul, South Korea*
[132] *Budker Institute for Nuclear Physics, Novosibirsk, Russia*
[133] *University of Zagreb, Zagreb, Croatia*
[134] *Physics Department, University of Rajasthan, Jaipur, India*
[135] *Institute of Theoretical Physics, University of Wroclaw, Wroclaw, Poland*
[136] *Laboratori Nazionali di Legnaro, INFN, Legnaro, Italy*
[137] *Hiroshima University, Hiroshima, Japan*
[138] *University of Kansas, Lawrence, Kansas, USA*
[139] *Centre de Calcul de l'IN2P3, Villeurbanne, France*

[*] Deceased.
[†] Permanent address: Konkuk University, Seoul, South Korea.